Journal of Fluids and Structures ▮ (▮▮▮▮) ▮▮▮–▮▮▮

Contents lists available at ScienceDirect

Journal of Fluids and Structures

journal homepage: www.elsevier.com/locate/jfs

Data-based hybrid reduced order modeling for vortex-induced nonlinear fluid–structure interaction at low Reynolds numbers

Daniele Gallardo, Riccardo Bevilacqua, Onkar Sahni *

Department of Mechanical, Aerospace and Nuclear Engineering (MANE), Rensselaer Polytechnic Institute, 110 8th street, Troy, NY 12180, USA

ARTICLE INFO

Article history:
Received 16 April 2013
Accepted 10 October 2013

Keywords:
Hybrid reduced order model
Data-based reduced order model
Cylinder in low Reynolds number regime
Fluid–structure interaction model
Computationally non-expensive FSI model

ABSTRACT

Fluid–structure interaction (FSI) phenomena are of significant importance in several engineering fields. Recently developed active flow control devices regulate the FSI in order to control the dynamic response of the structure that is involved. As a first step to use active control, computationally efficient reduced-order models are required. The reduced-order models must be able to predict the nonlinear structural dynamic response given an incoming flow condition. This paper presents a computationally efficient method for the construction of a hybrid reduced-order model for FSI problems based on data obtained through high-fidelity numerical simulations. The model splits the force and the structural dynamic response into two separate blocks and uses model reduction techniques to account for the flow field information. The current model is tested on a vibrating rigid cylinder submerged in a flow at low Reynolds number regime.

1. Introduction

Modeling fluid–structure interaction (FSI) phenomena is a problem of interest wherever the dynamics of structures is influenced by the surrounding flow and vice-versa. Practical cases where these interactions become critical are numerous and can be found in different engineering fields. In civil engineering the FSI phenomena become an issue for tall buildings, where the vibrations generated by the wind can cause discomfort to the residents on the higher floors or even structural damage to the building. Several studies on this problem have been published (Kareem et al., 1999; Lin et al., 2005) and some modeling techniques, e.g., using neural networks, have been proposed (Menicovich et al., 2012). A similar problem affects wind turbines, where the flow can cause the blades to vibrate and in some situations hysteresis in turbines' aerodynamic characteristics. These phenomena can cause mechanical fatigue of the blade which eventually translates into a reduction of the wind turbine life. An extended study on wind turbine FSI can be found by Bazilevs et al. (2011a, 2011b). Other studies that involve complex FSI that take place on offshore floating wind turbines have been proposed by Jonkman and Matha (2011). In the field of marine engineering, FSI occurs in marine risers that play an important role in the stability of marine structures, some studies on this topic have been proposed by Chaplin et al. (2005) and Hover et al. (1997). FSI models can also be used to improve performances of existing technologies, like the composite marine propeller described by Motley et al. (2009), or to assess the power output of novel energy technologies such as the wave energy extraction device described by Agamloh et al. (2008). FSI models are becoming increasingly important also in the biomedical field for studying

* Corresponding author. Tel.: +1 518 276 8560; fax: +1 518 276 4886.
E-mail addresses: gallad3@rpi.edu (D. Gallardo), bevilr@rpi.edu (R. Bevilacqua), sahni@rpi.edu (O. Sahni).

0889-9746/$ - see front matter © 2013 Elsevier Ltd. All rights reserved.
http://dx.doi.org/10.1016/j.jfluidstructs.2013.10.012

Nomenclature

A, B, C	linear model's state space matrices
a_j^k	predicted time coefficient of the jth mode at time t_k
$\tilde{a}_j^k$	measured time coefficient of the jth mode at time t_k
$\tilde{\mathbf{a}}_\mathbf{j}$	time history of the measured time coefficient of the jth mode
$\tilde{C}$	map between $\tilde{\mathbf{fr}}_{\mathbf{max}}$ and $\tilde{V}$, [Hz/(m/s)], $\tilde{C} \in R^{1\times 2l}$
c	structure damping coefficient [kg/s]
$d(t)$	structural displacement at time t [m]
$\dot{d}(t)$	structural velocity at time t [m/s]
$\ddot{d}(t)$	Structural acceleration at time t [m/s^2]
$\tilde{\mathbf{d}}$	time history of the structural displacement [m]
d_k	predicted structural displacement at t_k [m]
$\tilde{d}_k$	measured structural displacement at time t_k [m]
$\mathbf{e_k}$	predicted error between velocity vector field and projected states $\mathbf{x}_k$ at time t_k
$\tilde{\mathbf{e}}_\mathbf{k}$	measured error between $\tilde{\mathbf{v}}_k$ and the projected $\tilde{\mathbf{x}}_k$ at time t_k
$E\tilde{S}D_{\max}(k)$	maximum energy spectral density of force at time t_k [N^2/Hz]
$\tilde{\mathbf{F}}$	time history of the force [N]
F_k	modeled force at time t_k [N]
$\tilde{F}_k$	measured force at time t_k [N]
F_{M_k}	modeled force amplitude at time t_k [N]
$\tilde{\mathbf{F}}_u$	upper envelope of $\tilde{\mathbf{F}}$ [N]
f_M	fitting function that relates F_{M_k} with u_k and t_k
$f_{\max}$	Highest frequency in the wake [Hz]
f_{samp}	sampling frequency [Hz]
fr_{corr_k}	correcting term for the dominant frequency model at time t_k [Hz]
fr_k	dominant force frequency predicted by the linear model at time t_k [Hz]
$\hat{fr}_k$	compensated (or corrected) dominant force frequency at time t_k [Hz]
$\tilde{\mathbf{fr}}_{\mathbf{max}}$	time history of the dominant force frequency [Hz]
$\tilde{fr}_{\max}(k)$	measured dominant force frequency at time t_k [Hz]
g_{fr}^j	fitting function that relates a_j^k with u_k and time t_k
K	structure stiffness [N/m]
k	generic time step index
l	number of nodes in the mesh
M	total number of modes obtained through POD
m	structure mass [kg]
N	total number of samples gathered
P	number of modes actually used for reconstruction after truncation
p_{iq}	polynomial coefficients
r	number of states in the linear model
$\text{Re}_{\max}$	highest Reynolds number in the inflow condition of interest [dimensionless]
$\text{Re}_{\min}$	lowest Reynolds number in the inflow condition of interest [dimensionless]
S	number of samples contained in the moving sampling window [samples]
t	time [s]
$\tilde{\mathbf{u}}$	time history of the input flow condition (velocity) [m/s]
u_k	input flow condition at time t_k [m/s]
$\tilde{u}_k$	measured input flow condition at time t_k [m/s]
$\tilde{V}$	time history of the two-dimensional velocity vector field [m/s]
$\tilde{\mathbf{v}}_k$	measured velocity vector field at time t_k [m/s]
$\tilde{X}$	state trajectory of linear model given an input $\tilde{\mathbf{u}}$
$\mathbf{x}_k$	state vector of the linear model at time t_k
$\tilde{\mathbf{x}}_k$	state vector of the linear model at time t_k given an input $\tilde{u}_k$
z_k	state vector of the structural model
ΔRe	input flow condition resolution [dimensionless]
Δt	time step length [s]
Φ	map between $\tilde{X}$ and $\tilde{V}$ $\Phi \in R^{2l\times r}$
$\boldsymbol{\psi}_j$	generic jth mode
ω	angular frequency [rad/s]

the interactions that occur between soft tissues and blood. An example is presented in the work of Gerbeau et al. (2005), which uses medical images to build and validate the FSI model.

A complete review of the existing modeling techniques for general FSI problems is given by Dowell and Hall (2001) while a thorough review of the currents results and finding related to vortex-induced vibrations is given by Williamson and Govardhan (2004). Some models are developed for particular kinds of FSI problems, for example, the Stuart–Landau oscillator-based model developed by Thompson and Le Gal (2004, 2001) to study the FSI occurring in cylinder wakes. The vortex-induced vibrations that occur in the wake of cylinders are also reviewed in the work of Sarpkaya (2004). Another analytical model that presents a very rigorous mathematical formulation is the work of Benaroya and Gabbai (2007). As will be discussed later, from this study the current work borrows the idea of two separate models for the force exerted by the flow and for the structural dynamics, called "mechanical oscillators".

Alternative models are based on reduced order modeling (ROM) techniques that aim to condense the information contained in the flow field into a limited set of modes that are capable of reconstructing the flow field when combined properly and to be used in a feedback control. A characteristic of commonly used ROM techniques is their focus on the flow dynamics, rather than on the structural dynamics. Notable ROM work for the study of wake behind circular cylinder using proper orthogonal decomposition (POD) technique for mode decomposition has been done by Siegel et al. (2008, 2007),

Please cite this article as: Gallardo, D., et al., Data-based hybrid reduced order modeling for vortex-induced nonlinear fluid–structure interaction at low Reynolds numbers. Journal of Fluids and Structures (2013), http://dx.doi.org/10.1016/j.jfluidstructs.2013.10.012

Seidel et al. (2009) and Aradag et al. (2011). Other variations of POD technique include double-POD (DPOD) and filtered-POD. Another mode decomposition method used for flow problems is the dynamic mode decomposition (DMD) technique, developed by Schmid (2010). Particularly interesting from a control point of view is the work of Siegel et al. (2006) that applied feedback control of the cylinder wake, where structural motion is prescribed in order to change the wake flow condition.

Use of active flow control devices for FSI problems (where structural response is unknown a priori), makes it necessary to determine the dynamics by a computationally efficient ROM for a very broad set of inflow conditions that is of interest. This is because performing high-fidelity numerical simulations or experiments in real-time is not feasible. Furthermore, covering very large set of incoming flow conditions through high-fidelity numerical simulations would not be realistic due to their expensive nature. Similarly, carrying out experiments for a broad range of conditions would be impractical.

In this paper we present an efficient reduced-order modeling technique to determine the non-linear dynamic response of a structure due to the force exerted by a surrounding fluid in motion. In this technique the model is constructed or trained based on a dataset representative of the broad set of input conditions of interest. This dataset can be gathered through high-fidelity numerical simulations or experiments. In the current study we use high fidelity numerical simulations.

The model consists of two main blocks, as in the work of Benaroya and Gabbai (2007), with the main difference of having the two blocks constructed using gathered data instead of being derived with an analytical approach. The first block models the force exerted by the fluid on the structure (from now on referred to as *force model*), while the second block takes into account the dynamics of the structure and computes the structural response based on the modeled force from the first block (the second block is referred to as *structural model*).

The *force model* is further divided into two separate submodels, one modeling the frequency of the force exerted by the flow (from now on referred to as *frequency model*) and the other modeling the force amplitude (from now on referred to as *amplitude model*). The *frequency model* consists of a linear model (that relates the frequency of the force to the inflow velocity) along with a non-linear corrector that compensates for the possibly non-linear behavior due to the surrounding flow (which is based on the flow field). The structure of the *frequency model* is similar to the one developed by Ge and Wen (2011) for the study of the airflow in a contraction section. Our overall ROM technique is hybrid in nature in that it is composed of blocks and submodels as well as it combines a linear model with a non-linear corrector (for the frequency model).

A two-dimensional cylinder–fluid interaction in a flow at low Reynolds numbers has been chosen to demonstrate the applicability of the method. The cylinder is suspended on a mass-spring-damper system and only allowed to move in the vertical direction (i.e. it is constrained in the horizontal direction). This particular FSI case has been chosen because it is a well-known FSI problem for which both experimental (Anagnostopoulos and Bearman, 1992) and numerical (Bahmani and Akbari, 2011; Nomura, 1994) studies exist. Moreover, this FSI case has been chosen because it represents a very active field of research, for example see Satish et al. (2013) and Carmo et al. (2013).

In the current study, the dynamic behavior of the cylinder in the chosen flow regime is highly non-linear since the lock-in phenomenon is triggered, causing exponential growth in the cylinder's oscillations. The performance of the model has been evaluated and compared with the results obtained with high fidelity simulations.

The paper is organized as follows. Section 2 discusses different parts of the hybrid model. Section 3 describes the case study and compares the results from the hybrid model with high fidelity simulations. Section 4 draws the conclusions.

2. Hybrid reduced order model

The current ROM technique can be built using numerical or experimental data. In the current study numerical data has been used. The inflow conditions, represented by the Reynolds number, are the input while the output is the structural response due to the forces exerted by the fluid in motion.

In the current hybrid model the force exerted by the flow is applied at a single point on the suspended cylinder and it is assumed that the cylinder rigidly translates along the vertical direction (i.e., it is constrained in the horizontal direction).

The inflow conditions are defined with three key parameters:

- $\mathrm{Re}_{\min}$: Minimum Reynolds number
- $\mathrm{Re}_{\max}$: Maximum Reynolds number
- $\Delta\mathrm{Re}$: Resolution of Reynolds number

The minimum and maximum Reynolds number ($\mathrm{Re}_{\min}$ and $\mathrm{Re}_{\max}$ respectively) span the inflow condition of interest while $\Delta\mathrm{Re}$ defines the resolution of the inflow condition. Another important element for the data generation is the time resolution. A general idea of the highest frequency content of the phenomena $f_{\max}$ is needed in order to respect the minimum limit of sampling frequency due to the Nyquist–Shannon criterion (Shannon, 1949).

The current FSI model is split into two main parts; one modeling the force exerted by the flow on the structure (*force model*), and the other modeling the structural dynamic response (*structural dynamics model*), which depends on its dynamics parameters. The *force model* itself is made of two submodels, one modeling the frequency at which the force is exerted on the structure (*frequency model*) and the other modeling the amplitude of the force (*amplitude model*). These two

Please cite this article as: Gallardo, D., et al., Data-based hybrid reduced order modeling for vortex-induced nonlinear fluid–structure interaction at low Reynolds numbers. Journal of Fluids and Structures (2013), http://dx.doi.org/10.1016/j.jfluidstructs.2013.10.012

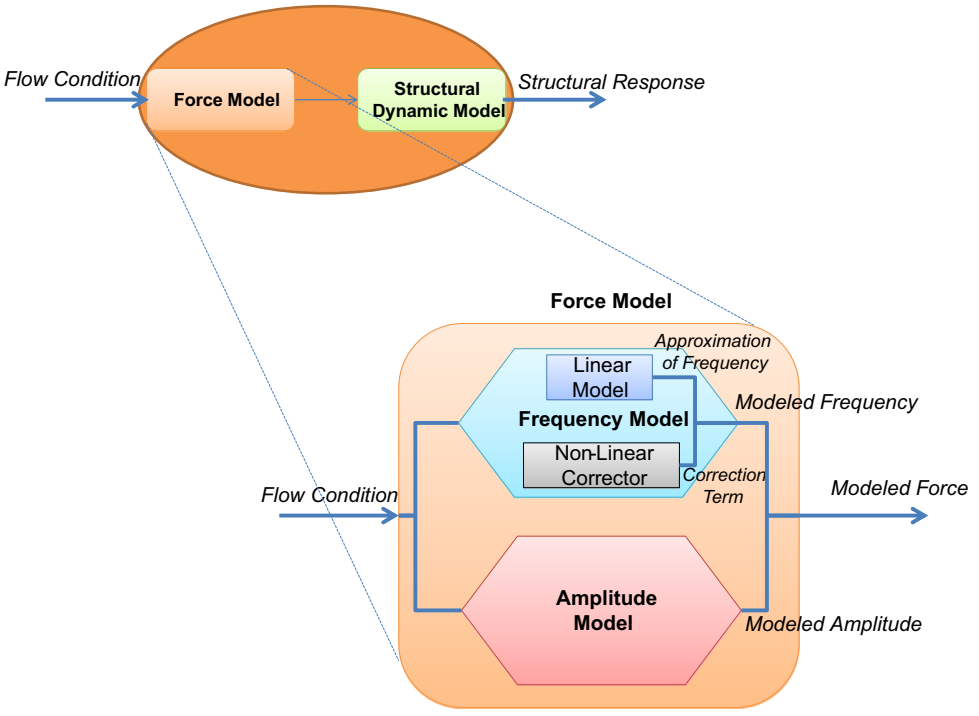

Fig. 1. Fluid–structure interaction model.

parts are combined and the resulting force signal is fed into the *structural dynamic model* to determine the dynamic response of the structure. The overall structure of the model is given in Fig. 1. The upper oval represents the overall model, composed of two blocks: (fluid) force model and a structural dynamic model. In the overall model, the input is the inflow condition (freestream velocity) and the output is the structural response (i.e., displacement). The box below the oval represents the force model with its two separate submodels representing the frequency model and the amplitude model. Additionally, the structure of the frequency model is composed of a linear model that is compensated by a non-linear corrector.

In the model there is no explicit feedback from the structural response to the (fluid) force signal but since the force model is developed using the information about the flow field along with the oscillation of the cylinder, this connection is implicitly captured. The frequency model consists of a linear, time-invariant (LTI) model, which relates the input conditions to the frequency, and also includes a non-linear corrector. The corrector is related to the velocity vector field and it compensates for the non-linearities in the surrounding flow dynamics.

In order to construct the current model, it is necessary to populate the following dataset:

- Time evolution of the input flow condition $\tilde{\mathbf{u}} = \left[\tilde{u}_1 \quad \tilde{u}_2 \quad \cdots \quad \tilde{u}_k \quad \cdots \quad \tilde{u}_N\right]$
- Time evolution of the structural displacement $\tilde{\mathbf{d}} = \left[\tilde{d}_1 \quad \tilde{d}_2 \quad \cdots \quad \tilde{d}_k \quad \cdots \quad \tilde{d}_N\right]$.
- Time evolution of the two-dimensional velocity vector field $\tilde{V} = \left[\tilde{\mathbf{v}}_1 \quad \tilde{\mathbf{v}}_2 \quad \cdots \quad \tilde{\mathbf{v}}_k \quad \cdots \quad \tilde{\mathbf{v}}_N\right]$.
- Time evolution of (fluid) force acting on the structure $\tilde{\mathbf{F}} = \left[\tilde{F}_1 \quad \tilde{F}_2 \quad \cdots \quad \tilde{F}_k \quad \cdots \quad \tilde{F}_N\right]$.

N is the total number of samples collected. The samples span the inflow conditions between $\mathrm{Re}_{\min}$ and $\mathrm{Re}_{\max}$ with a resolution $\Delta\mathrm{Re}$. The samples must be taken with a sampling frequency $f_{\mathrm{samp}} \geq 2f_{\max}$.

2.1. Force model

As shown in Fig. 1, the modeled force input is generated using the modeled force amplitude and frequency signals. This relationship is expressed as

$$F_k = F_{M_k} \sin(2\pi \hat{f} r_k t_k), \tag{2.1}$$

Please cite this article as: Gallardo, D., et al., Data-based hybrid reduced order modeling for vortex-induced nonlinear fluid–structure interaction at low Reynolds numbers. Journal of Fluids and Structures (2013), http://dx.doi.org/10.1016/j.jfluidstructs.2013.10.012

where F_k is the modeled force, F_{M_k} is the modeled force amplitude and $\hat{f}r_k$ is the modeled frequency; these are at a given time step $t_k = k\Delta t$, with Δt as the time interval between two consecutive time steps.

In order to determine a proper model for the force amplitude using the sampled force data $\tilde{\mathbf{F}}$, it is necessary to filter out the effects given by the oscillatory term in Eq. (2.1). These effects will be determined in the frequency model. The filtering is achieved by determining the upper envelope of the force data $\tilde{\mathbf{F}}_u$. The envelope is then used to fit a function $f_M(u_k, t_k)$ that relates the force amplitude to the input condition, as expressed in the following equation:

$$F_{M_k} = f_M(u_k, t_k). \tag{2.2}$$

The fitting function depends on the FSI problem analyzed and it must capture the behavior of the force amplitude given a certain inflow condition. As discussed in Section 3 and shown in Fig. 7, a polynomial of the 5th order (with respect to the input) can sufficiently approximate the changes in the force amplitude exerted on the cylinder.

For the frequency model, an understanding of the time evolution of the dominant frequency in the force signal is needed. Identifying the dominant frequency at any time point requires data from a local time window, i.e., some steps before and after the time of interest, containing $S+1$ samples. In this time window, the energy spectral density (ESD) is obtained through fast Fourier transformation (Marks, 2009) and performed with the purpose of determining the dominant force frequency $\tilde{f}r_{\max}(k)$ over time. The dominant frequency is the one associated with the maximum of the ESD distribution. This way for each time step $t_k$an associated dominant frequency $\tilde{f}r_{\max}(k)$ is determined. This is done according to the following relation:

$$E\tilde{S}D_{\max}(k) = \max(E\tilde{S}D(\omega)_k) = \max\left\{\frac{\Delta t}{2\pi}\left|\sum_{n=k-(S/2)}^{k+(S/2)} \tilde{F}_n e^{-i\omega n}\right|^2\right\} \rightarrow \tilde{f}r_{\max}(k). \tag{2.3}$$

Given the nature of the current method, frequency data will be available only from the $(1+(S/2))$th to the $(N-(S/2))$th time steps, which is sufficient for the current study. However, it is possible to use a skewed or one-sided time window at the ends of the time interval in order to determine the dominant frequency at all time steps from 1 to N.

The LTI model that is discrete in time is identified using a subspace identification method (Van Overschee and De Moor, 1993, 1994) with the dominant frequency data $\tilde{\mathbf{fr}}_{\mathbf{max}}$ as its output and the inflow condition $\tilde{\mathbf{u}}$ as its input that is of appropriate size (i.e., using the same number of element as in the dominant frequency vector). The identified LTI model has the following form:

$$\begin{aligned} \mathbf{x_{k+1}} &= A\mathbf{x_k} + Bu_k, \\ fr_k &= C\mathbf{x_k}. \end{aligned} \tag{2.4}$$

The state vector in LTI model, $\mathbf{x_k}$, is assumed to be relatively very low-dimensional (i.e. $\mathbf{x_k} \in R^r$). Instead of directly correlating the output of the linear model to the states, we suppose that there exists a correlation between the output frequency and the velocity vector field (a high-dimensional state vector, i.e. $\tilde{\mathbf{v}}_\mathbf{k} \in R^{2l}$ with $r \ll l$), expressed as

$$fr_k = \tilde{C}\tilde{\mathbf{v}}_\mathbf{k}. \tag{2.5}$$

This has a physical meaning since the changes in the velocity vector field influence the force frequency. It is possible to determine the matrix $\tilde{C}$ such that the error $||\tilde{\mathbf{fr}}_{\mathbf{max}} - \tilde{C}\tilde{V}||$ is minimized in a least square sense, where $\tilde{C} \in R^{1\times 2l}$. Since the output necessarily correlates to the states of the linear system, we assume that a map exists between the velocity vector field (a high-dimensional state vector) and the low-dimensional state vector as follows:

$$\mathbf{v_k} = \Phi\, \mathbf{x_k}. \tag{2.6}$$

Producing the state trajectory matrix $\tilde{X}$ using the LTI model with $\tilde{\mathbf{u}}$ as input, it is possible to determine the map Φ with a least square fit, where $\Phi \in R^{2l\times r}$. Rewriting Eq. (2.4) considering the correlations expressed in Eqs. (2.5) and (2.6) the frequency LTI model can be written as

$$\begin{aligned} \mathbf{x_{k+1}} &= A\mathbf{x_k} + Bu_k, \\ fr_k &= \tilde{C}\mathbf{v_k} = \tilde{C}\Phi\, \mathbf{x_k}. \end{aligned} \tag{2.7}$$

The linear model will only be able to predict the frequency of the force locally. In fact, because of the non-linearities, there is an error $\mathbf{e_k}$ between the mapped states and velocity vector field, which can be expressed as

$$\mathbf{e_k} = \mathbf{v_k} - \Phi\, \mathbf{x_k}. \tag{2.8}$$

Since it is impractical to use in a model all the information related to the high-dimensional velocity vector field, this error has to be computed in an alternate way. Using the state trajectory matrix $\tilde{X}$ and the velocity vector field matrix $\tilde{V}$, it is possible to determine the measured error $\tilde{\mathbf{e}}_\mathbf{k}$ for each time step, following Eq. (2.8). The measured error can be decomposed with the proper orthogonal decomposition (POD) method (Liang et al., 2002; Rowley et al., 2000) in a summation of M modes ψ_j (where M is the total number of temporal snapshots considered in POD). Each mode is properly scaled by their time coefficients $\tilde{a}_j^k$ resulting in

$$\tilde{\mathbf{e}}_\mathbf{k} = \sum_{j=1}^{M} \boldsymbol{\psi}_j \tilde{a}_\mathbf{j}^\mathbf{k}. \tag{2.9}$$

Please cite this article as: Gallardo, D., et al., Data-based hybrid reduced order modeling for vortex-induced nonlinear fluid–structure interaction at low Reynolds numbers. Journal of Fluids and Structures (2013), http://dx.doi.org/10.1016/j.jfluidstructs.2013.10.012

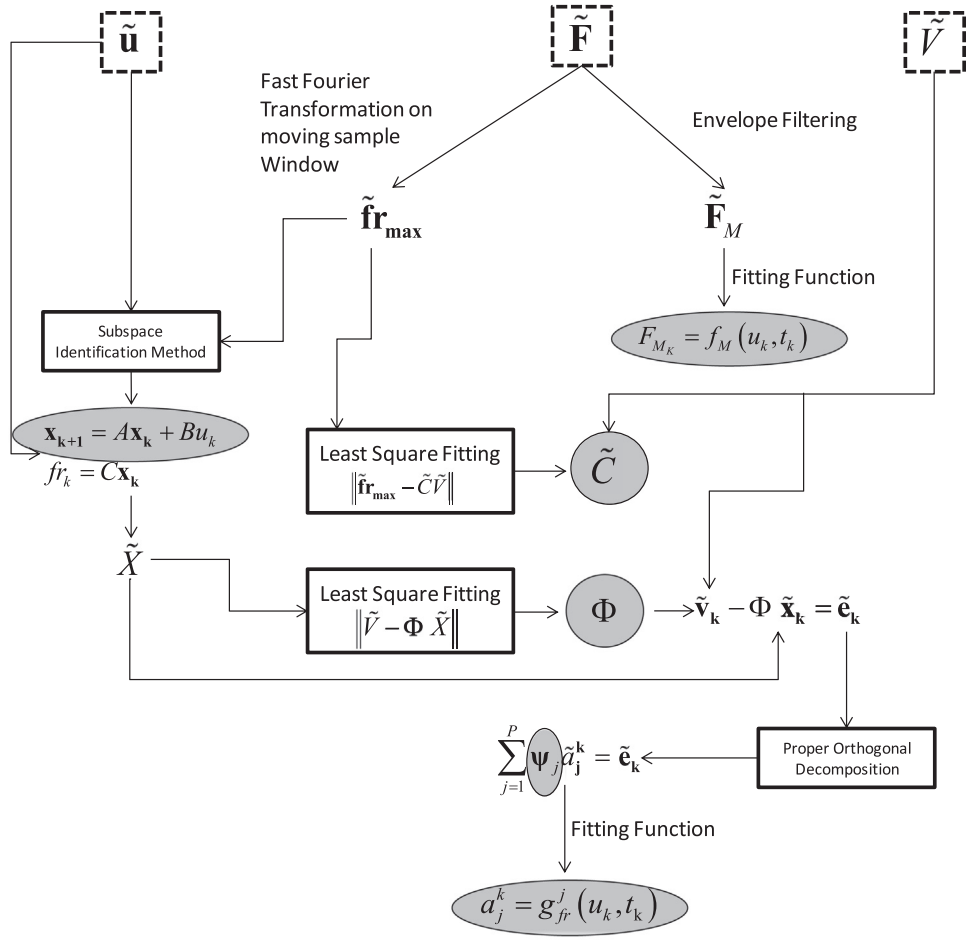

Fig. 2. Schematic representing the steps needed to build the hybrid reduced-order force model. In gray ovals and circles are the equations and variables used in the hybrid force model.

Since a truncation process takes place (only P modes out of the original M are selected), there is a difference between the theoretical error $\mathbf{e_k}$ and the reconstruction of the measured error $\tilde{\mathbf{e}}_\mathbf{k}$. The number of modes that has to be selected varies with the FSI problem at hand and can be determined by evaluating the energy associated with each mode. Assuming that P modes are sufficient to reconstruct the error (for example, they are assumed to be sufficient when the total captured energy is bigger than 98% of the total modal energy), it is possible to say that $\tilde{\mathbf{e}}_\mathbf{k} \cong \mathbf{e_k}$. After decomposing the measured error based on Eq. (2.9), a time evolution of each modal time coefficient $\tilde{\mathbf{a}}_j$ will be available. These time evolutions are used to train P fitting functions $g^j_{fr}(u_k, t_k)$ that relate the value of each modal time coefficient with the input condition and time step as

$$a^k_j = g^j_{fr}(u_k, t_k). \tag{2.10}$$

Using this set of P fitting functions, it is possible to determine the value of the modal time coefficients at a given input condition and time step, which determines the approximation to error due to the linear frequency model. Eq. (2.11) represents the linear model and its non-linear corrector fr_{corr_k} for determining the compensated (or corrected) dominant force frequency at a time step:

$$\hat{fr}_k = fr_k + fr_{\mathrm{corr}_k} = \tilde{C}\,\Phi\,\mathbf{x_k} + \tilde{C}\,\mathbf{e_k} = \tilde{C}\left(\Phi\,\mathbf{x_k} + \sum_{j=1}^{P} \boldsymbol{\psi}_j a^k_j\right). \tag{2.11}$$

The main steps described above are represented in Fig. 2.

To summarize, the force model expressed in Eq. (2.1) can be written in its extended form, as follows:

$$\mathbf{x_{k+1}} = A\mathbf{x_k} + Bu_k,$$

$$a^k_j = g^j_{fr}(u_k, t_k),$$

Please cite this article as: Gallardo, D., et al., Data-based hybrid reduced order modeling for vortex-induced nonlinear fluid–structure interaction at low Reynolds numbers. Journal of Fluids and Structures (2013), http://dx.doi.org/10.1016/j.jfluidstructs.2013.10.012

$$\hat{f}r_k = \tilde{C}\left(\Phi \mathbf{x_k} + \sum_{j=1}^{P} \psi_j a_j^k\right),$$
$$F_{M_k} = f_M(u_k, t_k),$$
$$F_k = F_{M_k} \sin(2\pi \hat{f}r_k t_k). \tag{2.12}$$

2.2. Structural dynamic model

The output of the force model is used, in cascade, as the input to the structural dynamic model (see Fig. 1). The model depends on the FSI problem analyzed. For the two-dimensional case involving rigid cylinder we choose a mass-spring-damper system with a concentrated force exerted by the fluid. The structural dynamic model does not explicitly affect the construction of the force model; however, it is accounted for implicitly (as discussed above).

The structural model is expressed as

$$m\ddot{d}(t) + c\dot{d}(t) + Kd(t) = F(t), \tag{2.13}$$

where m is the mass, c is the damping coefficient and K is the stiffness. $F(t)$ is the applied force while $d(t)$ represents the displacement of the rigid structure with respect to its initial position. Considering the forcing term as the force determined in Eq. (2.12) and representing the structural model in a discrete space state form, we obtain:

$$\mathbf{z}_{k+1} = \begin{bmatrix} 0 & 1 \\ \frac{K}{m} & \frac{c}{m} \end{bmatrix} \mathbf{z}_k + \begin{bmatrix} 0 \\ \frac{1}{m} \end{bmatrix} F_k,$$
$$d_k = \begin{bmatrix} 1 \\ 0 \end{bmatrix}^T \mathbf{z}_k, \tag{2.14}$$

where $\mathbf{z}_k$ is the state vector (two states for the mass-spring damper system, representing the displacement and the velocity of the structure, respectively). d_k represents the displacement at time t_k.

3. Model construction and results

3.1. FSI problem setup

The validity of the mathematical model derived in Section 2 was tested with a well-known FSI case (Anagnostopoulos and Bearman, 1992; Bahmani and Akbari, 2011; Nomura, 1994): a cylinder submerged into a flow at a low Reynolds number regime. In this particular setup, which is similar to the one analyzed by Anagnostopoulos and Bearman (1992), the cylinder is allowed to rigidly oscillate only along the cross-flow or vertical direction. Also, the cylinder has a mass m and is attached to a structure that introduces stiffness K and a damping c to its dynamics. The incoming flow has a free stream velocity $u(t)$. The cylinder has a diameter D. A representation of the setup is given in Fig. 3, while the values of m, K, c and D are reported in Table 1.

In the current study the goal is to characterize the cylinder's dynamic response when the incoming flow or free stream velocity changes dynamically and spans the region in which the lock-in phenomenon takes place (meaning a region where the vortex shedding frequency is close to the natural frequency of the structure). This particular region has been chosen because it presents highly non-linear dynamics and is a good test for our hybrid modeling technique. According to Anagnostopoulos and Bearman (1992), Bahmani and Akbari (2011) and Nomura (1994) the lock-in phenomena for a setup same as the one shown in Fig. 3 should occur at $105 \leq \mathrm{Re} \leq 115$.

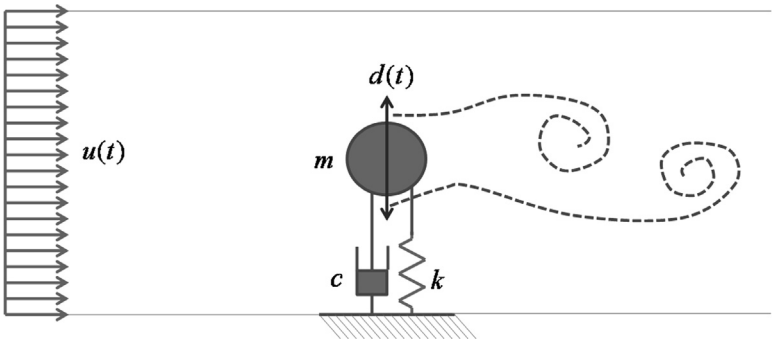

Fig. 3. Schematic of the FSI problem setup. The cylinder is allowed to move vertically.

Please cite this article as: Gallardo, D., et al., Data-based hybrid reduced order modeling for vortex-induced nonlinear fluid–structure interaction at low Reynolds numbers. Journal of Fluids and Structures (2013), http://dx.doi.org/10.1016/j.jfluidstructs.2013.10.012

Table 1
Values of the structural parameters.

Parameter	Value	Units
m	9.5328e−4	kg
K	1.8528	N/m
c	1.04e−4	kg/s
D	1.6e−3	m

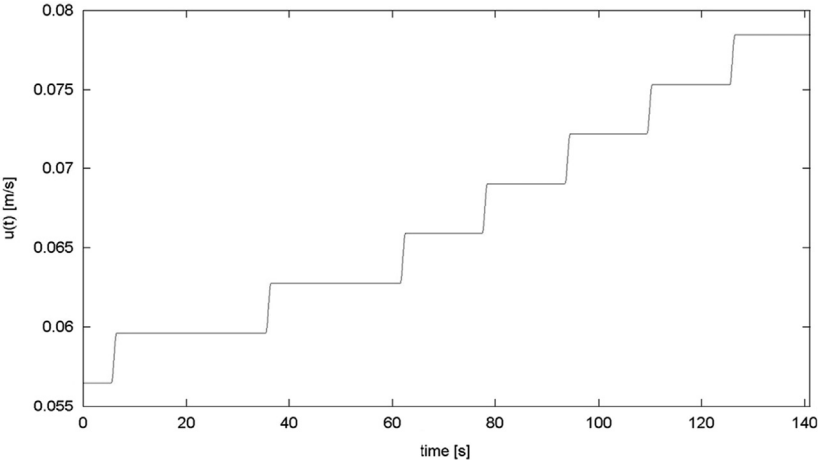

Fig. 4. Temporal evolution of the input flow velocity.

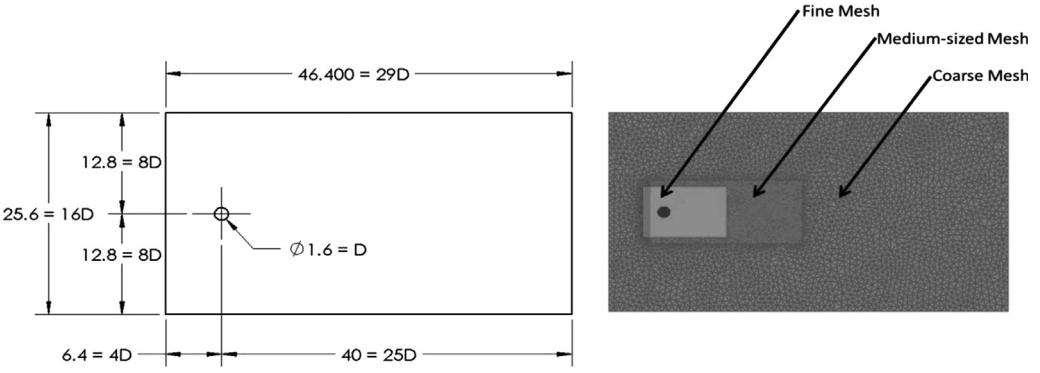

Fig. 5. Left: flow field dimensions. D is the diameter of the cylinder. All dimensions are in mm. Right: mesh with three different refinement zones.

3.2. High-fidelity numerical simulations

In order to generate the data needed for building the hybrid reduced-order model that was described in Section 2, high-fidelity numerical simulations were performed. Current simulations employed streamline upwind Petrov–Galerkin (SUPG) stabilization method for spatial discretization (Whiting and Jansen, 2001) and implicit time-integration based on generalized-alpha technique (Jansen et al., 1999). *AcuSolve*™ CFD software (Altair Engineering Inc., 2013) was used based on arbitrary Lagrangian–Eulerian (ALE) formulation. The inflow velocity was setup to change dynamically from Re 90 to Re 125, following the profile shown in Fig. 4. In this regime, there are negligible three-dimensional effects (Dowell and Hall, 2001), and for this reason, a two-dimensional simulation of the setup shown in Section 3.1 was created. A representation of the setup used in the numerical simulation is given in Fig. 5. The mesh for this problem consisted of unstructured triangles on the side plane, where three portions were considered, each one with a different mesh size. This was done because a relatively higher mesh resolution is needed closer to the cylinder for sufficient accuracy. Fig. 5 shows the mesh with three different refinement zones.

In numerical simulations, cylinder's dynamic response was recorded along with the force exerted on it as shown in Fig. 6. The simulations also recorded the flow field information.

The thick vertical line crossing the three graphs in Fig. 6 shows that the lock-in phenomenon which takes place at about Re = 100. This number is marginally lower than the ones found in Anagnostopoulos and Bearman (1992), Bahmani and

Please cite this article as: Gallardo, D., et al., Data-based hybrid reduced order modeling for vortex-induced nonlinear fluid–structure interaction at low Reynolds numbers. Journal of Fluids and Structures (2013), http://dx.doi.org/10.1016/j.jfluidstructs.2013.10.012

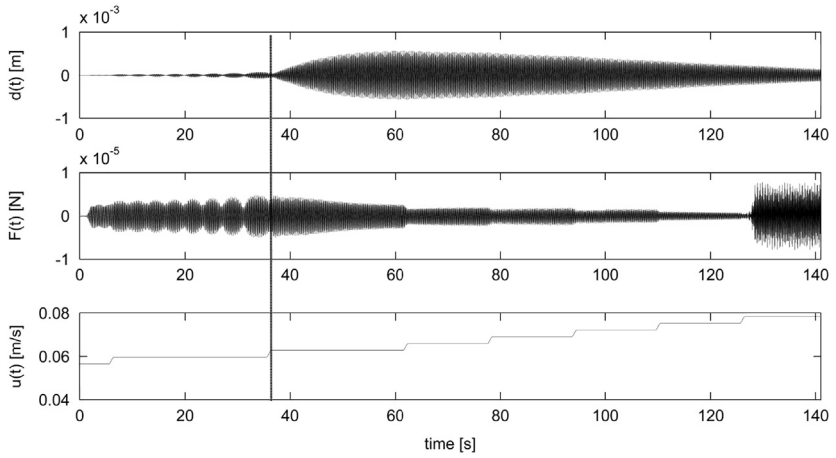

Fig. 6. Bottom: incoming flow velocity. Middle: force exerted by the flow on the cylinder along the cross-flow direction. Top: displacement $d(t)$ of the cylinder. The thick vertical line crossing the three graphs represents the time step where lock-in phenomenon is triggered, when the input flow condition reaches about Re = 100.

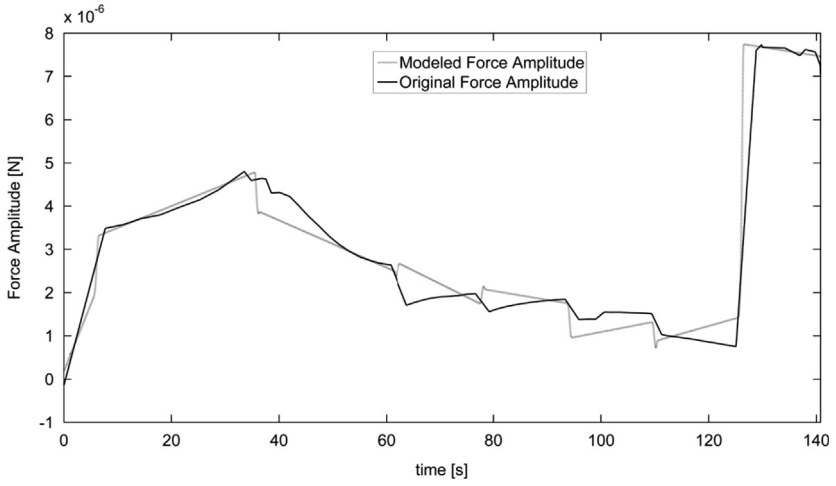

Fig. 7. Upper envelope of the original force signal from numerical simulations (continuous black line) and modeled force amplitude (continuous gray line).

Akbari (2011) and Nomura (1994), but the overall behavior is similar. Comparing the force profile with the displacement, the force amplitude does not appear to play an important role for the development of the exponential growth in the oscillations.

3.3. *Hybrid reduced order model*

The force amplitude was determined first for which the upper envelope of the force signal was used. This was used to fit a non-linear function as expressed in Eq. (2.2) that related the force amplitude with the input condition and time. Fig. 7 shows the envelope of the original signal and the modeled amplitude.

In this particular case the fit used is fifth order with respect to the input condition and first order with respect to time. This choice was considered because the relative L2 error was found to be low (as compared to other low-order choices).

The force signal was also analyzed to determine the dynamic dominant frequency, using a moving window as described in Section 2. The profile of the dominant frequency through this technique is shown in Fig. 8. This dominant frequency data was used to train a LTI model with two states $\mathbf{x_k} \in R^2$, using the inflow velocity as the input.

The state trajectory of the LTI model was mapped to the velocity vector field as in Eq. (2.6) and the error was decomposed using POD, as in Eq. (2.9). First nine modes were used to reconstruct the error in order to capture 98% of the energy. Their time coefficients were used to train nine non-linear functions to predict the value of the time coefficients depending on the value of the inflow velocity and time. The non-linear functions include fit based on fifth order with respect to the input and first order with respect to the time. As in the case of force amplitude, this choice was found to be sufficient. Fig. 9 shows the energy captured by the first 50 (POD) modes.

Using these functions, the LTI model was corrected as in Eq. (2.11). In order to improve the model, since the chosen case is extremely sensitive to frequency fluctuations, a filter has been introduced that assumes the frequency equal to the critical

Please cite this article as: Gallardo, D., et al., Data-based hybrid reduced order modeling for vortex-induced nonlinear fluid–structure interaction at low Reynolds numbers. Journal of Fluids and Structures (2013), http://dx.doi.org/10.1016/j.jfluidstructs.2013.10.012

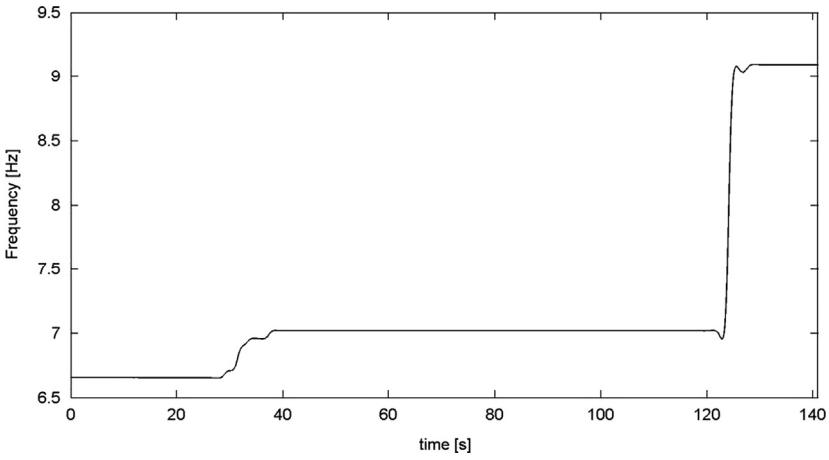

Fig. 8. Dominant frequency in the force signal from the numerical simulations.

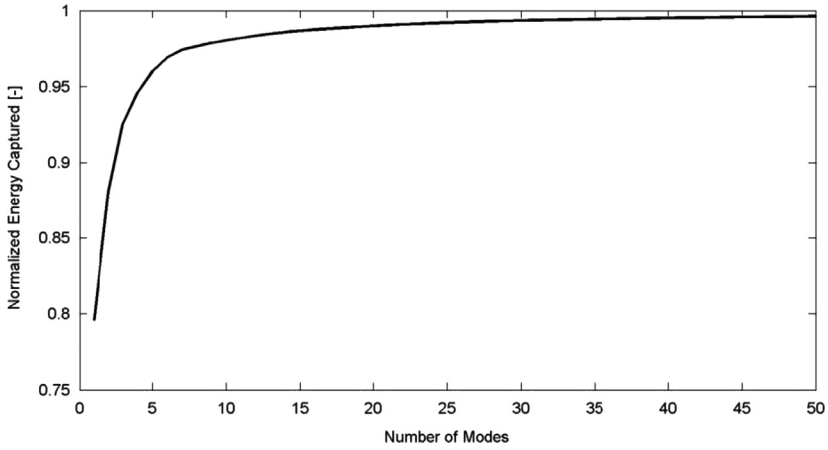

Fig. 9. Normalized energy captured by the first 50 modes.

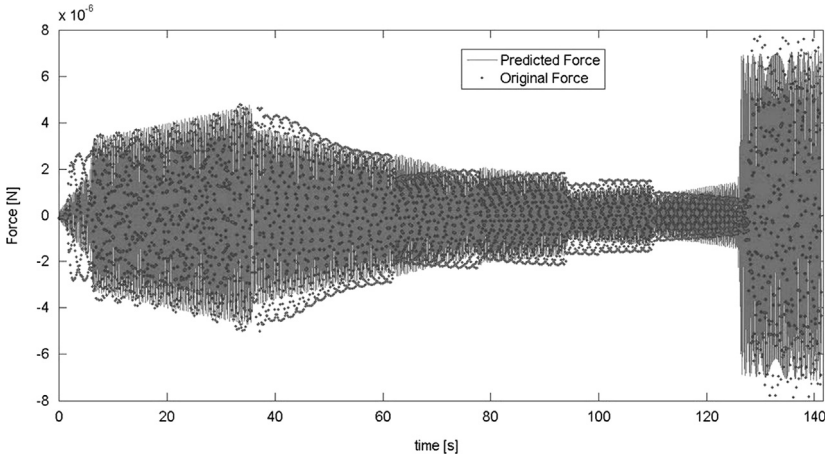

Fig. 10. Comparison of modeled force in gray line, and original force signal in black dots.

one (i.e., the natural frequency of the mass-spring-damper system) if the predicted frequency is within 5% of the critical value.

Combining the frequency model and the amplitude model, the complete force model was generated and compared to the one obtained through numerical simulation, as shown in Fig. 10. The modeled force signal was then used as the input signal to the structural dynamic model, which was created with the same structure as in Eq. (2.14) using the parameters listed in

Please cite this article as: Gallardo, D., et al., Data-based hybrid reduced order modeling for vortex-induced nonlinear fluid–structure interaction at low Reynolds numbers. Journal of Fluids and Structures (2013), http://dx.doi.org/10.1016/j.jfluidstructs.2013.10.012

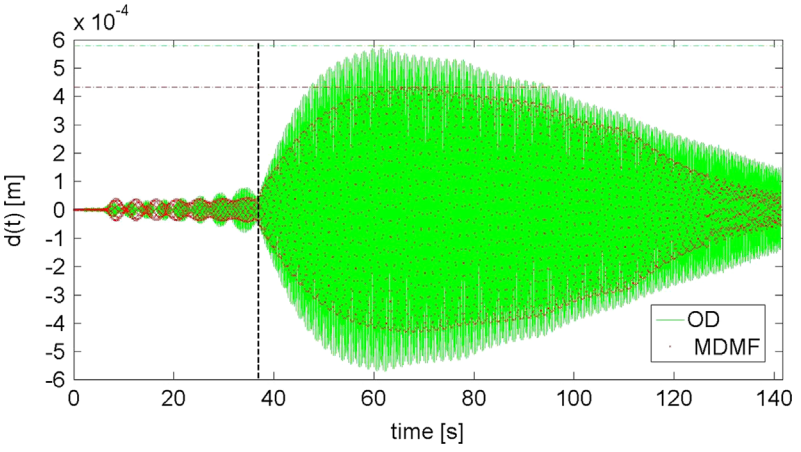

Fig. 11. Comparison of original displacement (OD) from high-fidelity numerical simulations (green line), and modeled displacement using modeled force signal (MDMF) in red dots. The horizontal lines correspond to the overall peak displacements: green horizontal line is at the OD maximum while red line at the MDMF maximum. The dashed vertical line represents the time at which the lock-in is triggered. (For interpretation of the references to color in this figure legend, the reader is referred to the web version of this article.)

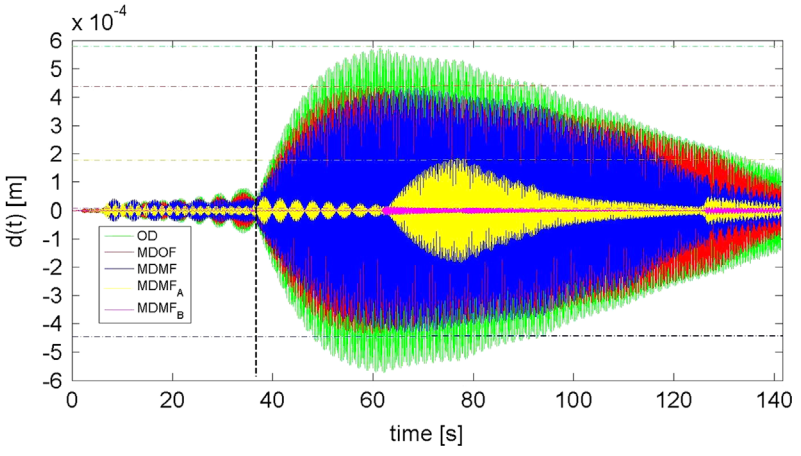

Fig. 12. Comparison of original displacement (OD) in green line, modeled displacement using original force signal (MDOF) in red line, modeled displacement using modeled force signal (MDMF) in blue line, modeled displacement using modeled force without using the non-linear corrector for frequency ($MDMF_A$) in yellow line, and modeled displacement using modeled force using only the LTI model for frequency ($MDMF_B$) in magenta line. Dotted horizontal lines represent the overall peak displacements for different displacement signals. The dashed black line represents the location at which the lock-in is triggered. (For interpretation of the references to color in this figure legend, the reader is referred to the web version of this article.)

Section 3.1. Fig. 11 shows the dynamic response of the cylinder in terms of its displacement in time $d(t)$ and the original displacement obtained through numerical simulations.

In order to determine the effects of different parts of the model, the following signals have also been used as input signals to the structural dynamic model:

- Original force signal from numerical simulations.
- Modeled force signal without using the non-linear corrector in the frequency model.
- Modeled force signal using only the LTI model for the frequency model.

The dynamic responses to these signals have been compared with the one obtained with the complete modeled force signal and are shown in Fig. 12.

Figs. 12 and 13 show that the modeled force signal and the original force signal produce consistently a remarkably similar dynamic response when used as an input to the structural dynamic model. This demonstrates that the hybrid force modeling technique successfully captures the behavior of the system in terms of the force exerted on the cylinder by the surrounding flow (both in terms of frequency and magnitude). A very similar time evolution of modeled and original force signals can be seen in Fig. 10. The modeled force closely follows the original force signal obtained in the numerical simulation. The few time locations that present minor differences correspond to the highest errors in the amplitude model,

Please cite this article as: Gallardo, D., et al., Data-based hybrid reduced order modeling for vortex-induced nonlinear fluid–structure interaction at low Reynolds numbers. Journal of Fluids and Structures (2013), http://dx.doi.org/10.1016/j.jfluidstructs.2013.10.012

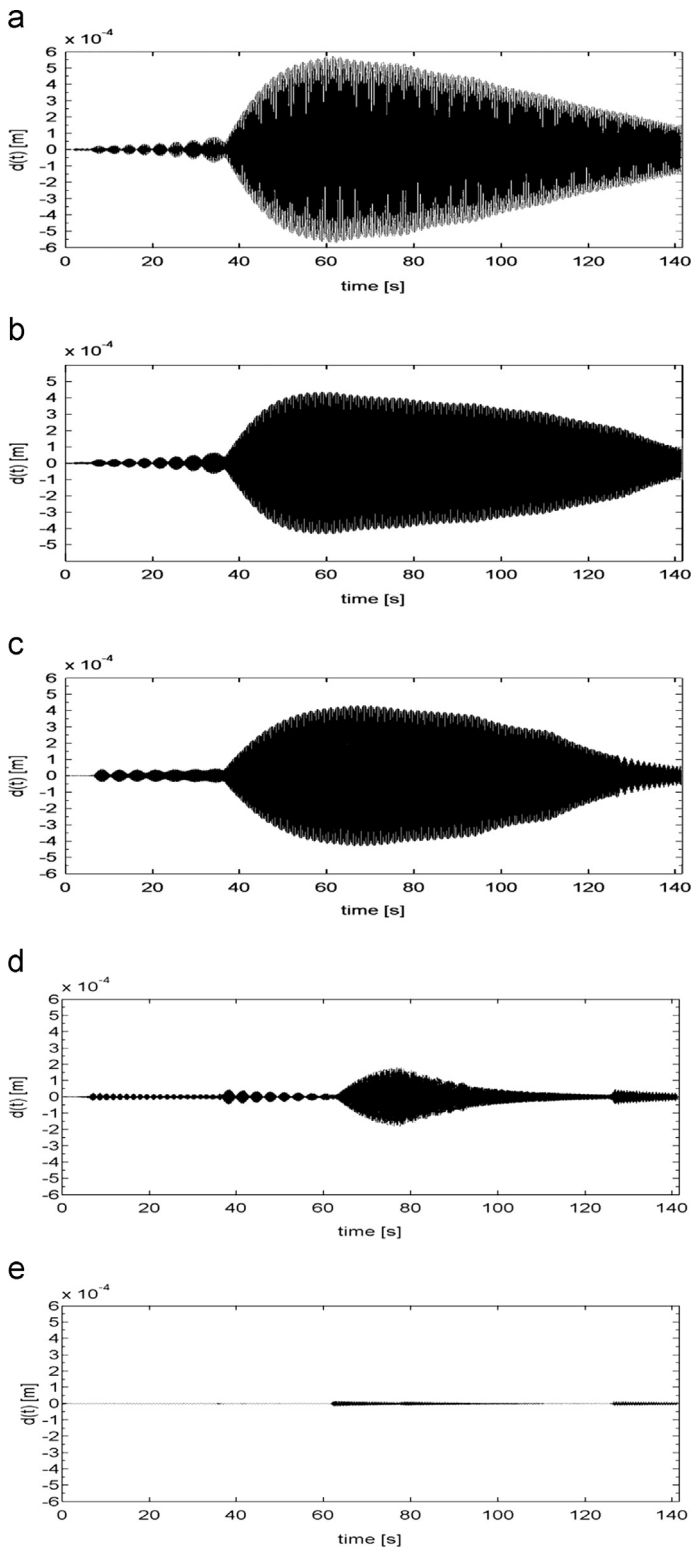

Fig. 13. (a) Original displacement (OD), (b) modeled displacement using original force signal (MDOF), (c) modeled displacement using modeled force signal (MDMF), (d) modeled displacement using modeled force without using the non-linear corrector for frequency ($MDMF_A$) and (e) modeled displacement using modeled force using only the LTI model for frequency ($MDMF_B$).

Please cite this article as: Gallardo, D., et al., Data-based hybrid reduced order modeling for vortex-induced nonlinear fluid–structure interaction at low Reynolds numbers. Journal of Fluids and Structures (2013), http://dx.doi.org/10.1016/j.jfluidstructs.2013.10.012

as it can be seen in Fig. 7. The differences between the modeled and the original force amplitude are caused by the non-linear transients due to the change in the input conditions that can be seen in the bottom of Fig. 6.

However, in Fig. 11, some differences are evident in the original displacement and the modeled displacement. It is particularly evident when looking at the horizontal lines at the overall peaks of the two displacements. Since the force model proved to be consistent, the cause of this difference lies in the structural dynamic model. In the current structural model, an element that needs to be considered is the effect of the surrounding fluid (e.g., see Chen et al., 1993, 1995). This is evident in Fig. 12 where the structural displacement in response to the original force signal produces the same behavior as the modeled force signal. Accounting for the effect of surrounding fluid in the parameters of the structural model will be the focus of future study. Fig. 12 also shows the importance of the non-linear corrector and of the inclusion of information related to the flow field into the frequency model: the structural response obtained using only a LTI model for the frequency model is poor and similarly unsatisfactory response is seen when the non-linear corrector term is not used.

Another interesting result that is evident from Figs. 12 and 13 is the implicit feedback of the structural response into the force model, mentioned in Section 2. Taking the original force signal from numerical simulations and using it as an input to the structural model gives a modeled structural response significantly similar to the original one from numerical simulations. This can be attributed to the fact that the force data implicitly contains information related to the structural response.

The hybrid model provides some information about the underlying flow physics. For example, in Fig. 12 it is evident that the model determines the right temporal location when the lock-in phenomenon is triggered, as shown by the vertical dotted line. Also, the temporal location of the peak modeled displacement is close to that of original displacement. In addition, the model captures the beating behavior of the system that is present in the initial phase (before lock-in is triggered).

4. Conclusions

The hybrid modeling technique presented in this paper uses gathered dataset in order to generate a reduced-order model for non-linear FSI phenomena. The main advantages of this modeling technique are that it results in a computationally efficient model as compared to those used in high fidelity numerical simulations and it determines the non-linear dynamic response of the structure (instead of focusing purely on the flow dynamics).

The modeling technique has been tested for predicting the dynamic response of a two-dimensional rigid cylinder that is suspended on a mass-spring damper system and immersed in a flow at low Reynolds number regime. The flow regime was chosen in order to trigger the lock-in phenomenon, causing an exponential growth in the cylinder's oscillations. Dataset needed for training the hybrid model was generated through high-fidelity numerical simulations.

The model demonstrated a successful prediction of the force exerted by the flow on the cylinder and the non-linear dynamic response of the structure. The lock-in phenomenon was captured by the model, with an exponential growth and closely follows the results from the high-fidelity numerical simulations.

References

Agamloh, E.B., Wallace, A.K., Von Jouanne, A., 2008. Application of fluid–structure interaction simulation of an ocean wave energy extraction device. Renewable Energy 33, 748–757.

Altair Engineering Inc., 2013. AcuSolve™ CFD software, 23 September 2013. ⟨http://www.altairhyperworks.it/Product,54,AcuSolve.aspx?AspxAutoDetectCookieSupport=1⟩.

Anagnostopoulos, P., Bearman, P.W., 1992. Response characteristics of a vortex-excited cylinder at low Reynolds numbers. Journal of Fluids and Structures 6, 39–50.

Aradag, S., Siegel, S., Seidel, J., Cohen, K., McLaughlin, T., 2011. Filtered POD-based low dimensional modeling of the 3D turbulent flow behind a circular cylinder. Numerical Methods in Fluids 66, 1–16.

Bahmani, M.H., Akbari, M.H., 2011. Response characteristic of a vortex-excited circular cylinder in laminar flow. Journal of Mechanical Science and Technology 25, 125–133.

Bazilevs, Y., Hsu, M.C., Akkerman, I., Wright, S., Takizawa, K., Henicke, B., Spielman, T., Tezduyar, T.E., 2011a. 3D simulation of wind turbine rotors at full scale. Part I: geometry modeling and aerodynamics. International Journal of Numerical Methods in Fluids 65, 207–235.

Bazilevs, Y., Hsu, M.C., Kiendi, J., Wuchner, R., Bletzinger, K.U., 2011b. 3D simulation of wind turbine rotors at full scale. Part II: fluid–structure interaction modeling with composite blades. International Journal of Numerical Methods in Fluid 65, 236–253.

Benaroya, H., Gabbai, R.D., 2007. Modeling vortex-induced fluid–structure interaction. Philosophical Transactions of the Royal Society 366, 1231–1274.

Carmo, B.S., Assi, G.R.S., Meneghini, J.R., 2013. Computational simulation of the flow-induced vibration of a circular cylinder subjected to wake interference. Journal of Fluids and Structures 41, 99–108.

Chaplin, J.R., Bearman, P.W., Huera Huarte, F.J., Pattenden, R.J., 2005. Laboratory measurements of vortex-induced vibrations of vertical tension risers in a stepped current. Journal of Fluids and Structures 21, 3–24.

Chen, S.S., Zhu, S., Cai, Y., 1995. An unsteady flow theory for vortex-induced vibration. Journal of Sound and Vibration 184, 73–92.

Chen, S.S., Zhu, S., Jendrzejczyk, J.A., 1993. Motion-dependent fluid forces acting on tube arrays in crossflow. Argonne National Laboratory Report ANL-93/15.

Dowell, E.H., Hall, K.C., 2001. Modeling of fluid–structure interaction. Annual Review of Fluid Mechanics 33, 445–490.

Ge, X., Wen, J.T., 2011. Hybrid model reduction for compressible flow controller design. In: Proceedings of the 50th IEEE Conference on Decision and Control and European Control Conference (CDC-ECC). Orlando, FL, USA, December 12–15, 2011.

Gerbeau, J.F., Vidrascu, M., Frey, P., 2005. Fluid structure interaction in blood flows on geometries based on medical imaging. Computers & Structures 83, 155–165.

Hover, F.S., Miller, S.N., Triantafyllou, M.S., 1997. Vortex-induced vibration of marine cables: experiments using force feedback. Journal of Fluids and Structures 11, 307–326.

Jansen, K.E., Whiting, C.H., Hulbert, G.M., 1999. A generalized-alpha method for integrating the filtered Navier–Stokes equations with a stabilized finite element method. Computer Methods in Applied Mechanics and Engineering 190, 305–319.

Jonkman, J.M., Matha, D., 2011. Dynamics of offshore floating wind turbines-analysis of three concepts. Journal of Wind Energy 14, 557–569.

Please cite this article as: Gallardo, D., et al., Data-based hybrid reduced order modeling for vortex-induced nonlinear fluid–structure interaction at low Reynolds numbers. Journal of Fluids and Structures (2013), http://dx.doi.org/10.1016/j.jfluidstructs.2013.10.012

Kareem, A., Kijewski, T., Tamura, Y., 1999. Mitigation of motions of tall buildings with specific examples of recent applications. Journal of Wind and Structures 2, 201–251.
Liang, Y.C., Lee, H.P., Lim, S.P., Lin, W.Z., Lee, K.H., Wu, C.G., 2002. Proper orthogonal decomposition and its applications—Part I: theory. Journal of Sound and Vibration 252, 527–544.
Lin, N., Letchford, C., Tamura, Y., Liang, B., Nakamura, O., 2005. Characteristics of wind forces acting on tall buildings. Journal of Wind Engineering and Industrial Aerodynamics 93, 217–242.
Marks II, R.J., 2009. Handbook of Fourier Analysis and its Applications. Oxford University Press.
Menicovich, D., Gallardo, D., Bevilacqua, R., Vollen, J.O., 2012. Generation and integration of an aerodynamic performance data-base within the concept design phase of tall buildings. In: Proceedings of the 2012 ACADIA Conference: Synthetic Digital Ecologies, San Francisco, October 2012.
Motley, M.R., Liu, Z., Young, Y.L., 2009. Utilizing fluid–structure interactions to improve energy efficiency of composite marine propellers in spatially varying wake. Journal of Composite Structures 90, 304–313.
Nomura, T., 1994. ALE finite element computations of fluid–structure interaction problems. Computer Methods in Applied Mechanics and Engineering 112, 291–308.
Rowley, C.W., Colonius, T., Murray, R.M., 2000. POD based models of self-sustained oscillations in the flow past and open cavity. In: Proceedings of the 6th AIAA/CEAS Aeroacoustics Conference.
Sarpkaya, T., 2004. A critical review of the intrinsic nature of vortex-induced vibrations. Journal of Fluids and Structures 19, 389–447.
Satish, P., Patwardhan, S.S., Ramesh, O.N., 2013. Effect of steady rotation on low Reynolds number vortex shedding behind a circular cylinder. Journal of Fluids and Structures 41, 175–186.
Schmid, P.J., 2010. Dynamic mode decomposition of numerical and experimental data. Journal of Fluid Mechanics 656, 5–28.
Seidel, J., Siegel, S., Fagley, C., Cohen, K., McLaughlin, T., 2009. Feedback control of a circular cylinder wake. Journal of Aerospace Engineering. 223, 379–392.
Shannon, C.E., 1949. Communication in the presence of noise. Proceedings of Institute of Radio Engineers 37, 10–21.
Siegel, S.G., Seidel, J., Fagley, C., Luchtenburg, D.M., Cohen, K., McLaughlin, T., 2008. Low-dimensional modeling of a transient cylinder wake using double proper orthogonal decomposition. Journal of Fluid Mechanics 610, 1–42.
Siegel, S.G., Cohen, K., Seidel, J., McLaughlin, T., 2007. State estimation of transient flow fields using double proper orthogonal decomposition (DPOD). In: King, R. (Ed.), Active Flow Control, Springer, Berlin, pp. 105–118.
Siegel, S., Cohen, K., McLaughlin, T., 2006. Numerical simulations of a feedback-controlled circular cylinder wake. AIAA Journal 44, 1266–1276.
Thompson, M.C., Le Gal, P., 2004. The Stuart–Landau model applied to wake transition revisited. European Journal of Mechanics—B/Fluids 23, 219–228.
Thompson, M.C., Le Gal, P., 2001. Application of the forced Stuart–Landau model to cylinder wake oscillation. In: Proceedings of the 14th Australian Fluid Mechanics Conference, Adelaide, Australia, December 2001.
Van Overschee, P., De Moor, B., 1994. N4SID: subspace algorithms for the identification of combined deterministic-stochastic systems. Automatica, Special Issue on Statistical Signal Processing and Control 30, 75–93.
Van Overschee, P., De Moor, B., 1993. N4SID: numerical algorithms for state space subspace system identification. In: Proceeding of the 12th IFAC World Congress, vol. 7, pp. 361–364.
Whiting, C.H., Jansen, K.E., 2001. A stabilized finite element method for the incompressible Navier–Stokes equations using a hierarchical basis. International Journal of Numerical Methods in Fluids 35, 93–116.
Williamson, C.H.K., Govardhan, R., 2004. Vortex-induced vibrations. Annual Review of Fluid Mechanics 36, 413–455.

Please cite this article as: Gallardo, D., et al., Data-based hybrid reduced order modeling for vortex-induced nonlinear fluid–structure interaction at low Reynolds numbers. Journal of Fluids and Structures (2013), http://dx.doi.org/10.1016/j.jfluidstructs.2013.10.012